

An efficient γ -model BGK scheme for multicomponent flows on unstructured meshes

Song Jiang Guoxi Ni*

LCP, Institute of Applied Physics and Computational Mathematics
P.O. Box 8009, Beijing 100088, China.
E-mail: jiang@iapcm.ac.cn, gxni@iapcm.ac.cn

Abstract

Based on the γ -model, the BGK scheme and the time-dependent gas distribution function, we present an efficient second-order gas-kinetic BGK scheme for compressible multicomponent flows on unstructured meshes. The second-order accuracy of the scheme is achieved by including slopes in the reconstruction step and the efficiency lies in the fact that the slopes in a cell are constructed by using the information in the cell only. Using the explicitly constructed time-dependent gas distribution function, we can obtain in addition the values of the flow variables at cell edges of the cell, which together with the cell averaged values make it possible to construct the slopes of the flow variables in the cell, avoiding the use of the values from neighboring cells in the usual process. Thus, with the stencil of a first-order scheme, we construct a second-order gas-kinetic scheme. Numerical examples illustrate the accuracy and efficiency of the scheme.

Classification (2000): 76M25, 65M99

Keywords: Multicomponent flows, efficient 2nd-order BGK scheme, γ -model, unstructured meshes

1 Introduction

In recent years, the development of Boltzmann-type schemes has attracted much attention. The success of such schemes has appeared in a wide range of applications, see [13, 14, 6, 16] for example. Among the Boltzmann-type schemes, the equilibrium-flux method (EFM) has been intensively studied [18]. EFM is flux splitting and is also referred to as a kinetic flux vector splitting (KFVS) scheme. With the inclusion of a Boltzmann collision model, the BGK model, in the flux evaluation process, the gas-kinetic BGK scheme has been proposed in [17, 24] (also see the survey article [25]). The BGK scheme differs from the KFVS method mainly in the inclusion of particle collisions in the gas evolution stage. Instead of solving the collisionless Boltzmann equation, the BGK scheme uses a collisional BGK model which approximates the Boltzmann collision operator when it is near equilibrium. Since the gas evolution process is associated with a relaxation process, i.e., from a non-equilibrium state to an equilibrium one, the entropy condition is satisfied by the BGK scheme. Once the physical structure can be well resolved by the numerical cell size, the BGK scheme automatically gives an accurate compressible Navier-Stokes solution in smooth regions, while in the discontinuous regions, the delicate dissipative mechanism in the BGK scheme generates a stable and crisp shock transition.

Numerical schemes for multicomponent flows associated with discontinuities and shock waves have been one of the most important topics in computational fluid dynamics. In the last decades great progress has been made, and a number of schemes have been proposed in the literature. Among them are methods which use an extended conservative system of governing equations, where additional conservation

*Corresponding author

equations are introduced to the original fluid dynamical equations to describe the conservation of parameters such as the level set functions, the mass fractions and the ratio of specific heats (γ -model) in the mixture, see [1, 9, 21] and among others. In order to maintain pressure equilibrium and positivity of the mass fractions, and eliminate spurious oscillations and computational inaccuracy near interfaces which are observed in some numerical computations obtained using these conservative methods, several non-conservative approaches to capture the contact discontinuities using an additional non-conservative governing equation are proposed, see [1, 22, 23] for example.

In [7], the authors of this paper proposed a first-order gas-kinetic BGK scheme on structured meshes for compressible multicomponent flows by incorporating a conservative γ -model given in [1] into the BGK scheme introduced in [17, 25]. The reason why we used the γ -model to capture the motion of interfaces is that in the framework of the BGK scheme and the process recovering the original equations by using local equilibrium states, for multicomponent fluids, the γ -model in the conservative form, which governs the motion of interfaces, can be (easily) incorporated in the BGK scheme. In [8] the authors extended the first-order γ -model BGK scheme proposed in [7] to the second-order one on structured meshes.

In this paper we construct an efficient second-order gas-kinetic BGK scheme for compressible multicomponent flows on unstructured meshes, extending thus the scheme of [8] to unstructured meshes. Furthermore, our scheme is computationally cheap and efficient. For the sake of clear presentation, we will restrict the construction of our scheme in two spatial dimensions only. However, the scheme of this paper can be extended to three spatial dimensions without any essential difficulties. The basic idea in the construction of our efficient kinetic scheme lies in that we can extract more information from the time-dependent gas distribution function within a cell which, together with the cell averaged values of the flow variables, makes it possible to obtain slopes of the flow variables in the cell. More precisely, at a cell interface, with the help of the explicitly constructed gas distribution function f we can evaluate not only the fluxes at a time step but also the value of the flow variables at the next time step. Thus, we can update the slopes by using the cell averaged value and the cell interface value of the flow variables in a cell. Therefore, with the stencil of a first-order scheme, we can construct a second-order gas-kinetic scheme. This avoids using the value of the conservative variables from appropriate neighboring cells in the construction of the slopes in the usual process (see [11, 14] for example). Consequently, we get an efficient discontinuous gas kinetic BGK scheme, which is computationally cheap, efficient and easy in coding. As is well-known, it is sometimes very difficult to choose a suitable stencil to construct slopes of the flow variables on unstructured meshes. We mention that in [15] a similar idea was used to construct kinetic schemes for steady and unsteady single-component flows on unstructured meshes.

This paper is organized as follows: In section 2, the gas-kinetic γ -BGK model for compressible multicomponent flows is presented. Section 3 is devoted to the construction of the efficient second-order kinetic scheme on unstructured meshes. In Section 4 we present some numerical examples to validate our scheme in the numerical simulation of compressible multicomponent fluids. A conclusion remark is given in the last section.

2 γ -Based BGK model for compressible flows

In this section, we derive the γ -based BGK model in two spatial dimensions. In [1] Abgrall introduced a non-conservative γ -model approach to capture contact discontinuities of two fluids using an additional non-conservative governing equation for the specific heat ratio γ in two spatial dimensions:

$$\frac{\partial}{\partial t} \left(\frac{1}{\gamma - 1} \right) + U \frac{\partial}{\partial x} \left(\frac{1}{\gamma - 1} \right) + V \frac{\partial}{\partial y} \left(\frac{1}{\gamma - 1} \right) = 0, \quad (2.1)$$

where U and V are the macroscopic velocities in x - and y -directions respectively. According to the analysis in [1], pressure equilibrium across an interface can be achieved using the equation (2.1), while an earlier γ -model scheme [21, 9] uses γ instead of $1/(\gamma - 1)$ and may result in pressure oscillations in the vicinity of the interface. We should point out here that the equation (2.1) is actually derived for a

scheme of Godunov-type (cf. [1]). For the scheme of the present paper, however, the numerical examples show that the equation (2.1) performs better than the earlier γ -model. Hence, we use (2.1) in our scheme for multifluid computations.

The equation (2.1) can be easily written in the following conservation form, using the conservation law of mass

$$\frac{\partial}{\partial t} \left(\frac{\rho}{\gamma-1} \right) + \frac{\partial}{\partial x} \left(\frac{\rho U}{\gamma-1} \right) + \frac{\partial}{\partial y} \left(\frac{\rho V}{\gamma-1} \right) = 0. \quad (2.2)$$

Next, we add (2.2) to the Euler equations and discuss the corresponding BGK model from which the Euler equations coupled with (2.2) can be recovered. The reason why we use the conservative form (2.2) instead of the non-conservative form (2.1) is that (2.2) can be easily incorporated in the framework of the BGK scheme.

The BGK model in two spatial dimensions can be written as (see, e.g., [2, 3, 26])

$$f_t + u f_x + v f_y = \frac{g - f}{\tau}, \quad (2.3)$$

where f is the gas distribution function and g is the equilibrium state approached by f , (u, v) is the particle velocity, both f and g are functions of x, y, t, u, v and the internal variable ξ, z , and the internal variable z is related to γ , the particle collision time τ is related to the viscosity and the heat conductivity coefficients. We should point out here that the dependence of f on the additional variable z makes it possible to recover the extended Euler equations (2.6) in which an interface is captured by using the equation (2.2). The equilibrium state g is usually assumed to be a Maxwellian distribution. In order to recover the extended Euler equations (2.6), the Maxwellian distribution should have the form:

$$g = \rho \left(\frac{\lambda}{\pi} \right)^{\frac{K+3}{2}} e^{-\lambda((u-U)^2 + (v-V)^2 + \xi^2 + (z-Z)^2)}, \quad (2.4)$$

where ρ is the macroscopic density, $Z = 1/(\gamma-1)$ is related to the equation (2.2), and $\lambda = m/(2kT)$ with m being the molecular mass, k is the Boltzmann constant and T is the macroscopic temperature. The total number of degree of freedom K in ξ is equal to $(5-3\gamma)/(\gamma-1)+1$, and ξ^2 denotes $\xi^2 = \xi_1^2 + \xi_2^2 + \dots + \xi_K^2$. The relation between the mass ρ , the momentum $\rho U, \rho V$, the energy E , ρZ and the distribution function is given by

$$(\rho, \rho U, \rho V, E, \rho Z)^T = \int \psi f d\Xi, \quad (2.5)$$

where

$$\psi = (\psi_1, \psi_2, \psi_3, \psi_4, \psi_5)^T = \left(1, u, v, \frac{1}{2}(u^2 + v^2 + \xi^2), z \right)^T$$

and $d\Xi = dudvdz d\xi$ is the volume element in the phase space with $d\xi = d\xi_1 \dots d\xi_K$.

Since the mass, the momentum and the energy are conservative during particle collisions, f and g satisfy the conservation constraints

$$\int (g - f) \psi_\alpha d\Xi = 0, \quad \alpha = 1, 2, 3, 4, 5$$

at any point in space and time.

For a local equilibrium state with $f = g$, the extended Euler equations can be obtained by taking the moments of ψ to the equation (2.3). This yields

$$\int \psi_\alpha (g_t + u g_x + v g_y) d\Xi = 0, \quad \alpha = 1, 2, 3, 4, 5,$$

and the corresponding extended Euler equations (coupled with (2.2)) are

$$\begin{pmatrix} \rho \\ \rho U \\ \rho V \\ E \\ \rho Z \end{pmatrix}_t + \begin{pmatrix} \rho U \\ \rho U^2 + p \\ \rho UV \\ (E + p)U \\ \rho ZU \end{pmatrix}_x + \begin{pmatrix} \rho V \\ \rho UV \\ \rho V^2 + p \\ (E + p)V \\ \rho ZV \end{pmatrix}_y = 0, \quad (2.6)$$

where $E = \frac{1}{2}\rho(U^2 + V^2 + \frac{K+2}{2\lambda})$ is the total energy and $p = \rho/(2\lambda)$ is the pressure.

To the first order of τ , the Chapman-Enskog expansion gives $f = g - \tau(g_t + ug_x + vg_y)$. We take the moments of ψ again to the equation (2.3) with this f to get the following compressible Navier-Stokes equations with a dynamic viscous coefficient $\mu = \tau p$, coupled with (2.2),

$$\begin{pmatrix} \rho \\ \rho U \\ \rho V \\ E \\ \rho Z \end{pmatrix}_t + \begin{pmatrix} \rho U \\ \rho U^2 + p \\ \rho UV \\ (E + p)U \\ \rho ZU \end{pmatrix}_x + \begin{pmatrix} \rho V \\ \rho V \\ \rho V^2 + p \\ (E + p)V \\ \rho ZV \end{pmatrix}_y = \begin{pmatrix} 0 \\ s_{1x} \\ s_{2x} \\ s_{3x} \\ s_{4x} \end{pmatrix}_x + \begin{pmatrix} 0 \\ s_{1y} \\ s_{2y} \\ s_{3y} \\ s_{4y} \end{pmatrix}_y \quad (2.7)$$

where

$$\begin{aligned} s_{1x} &= \tau p \left[2 \frac{\partial U}{\partial x} - \frac{2}{K+2} \frac{\partial U}{\partial x} + \frac{\partial V}{\partial y} \right], \\ s_{2x} &= \tau p \left[\frac{\partial V}{\partial x} + \frac{\partial V}{\partial y} \right], \\ s_{3x} &= \tau p \left[2U \frac{\partial U}{\partial x} + V \left(\frac{\partial V}{\partial x} + \frac{\partial U}{\partial y} \right) - \frac{2U}{K+2} \left(\frac{\partial U}{\partial x} + \frac{\partial V}{\partial y} \right) + \frac{K+4}{4} \frac{\partial}{\partial x} \left(\frac{1}{\lambda} \right) \right], \\ s_{4x} &= \tau p \frac{\partial Z}{\partial x}, \\ s_{1y} &= \tau p \left[2 \frac{\partial U}{\partial y} + \frac{\partial V}{\partial x} \right], \\ s_{2y} &= \tau p \left[\frac{\partial V}{\partial y} \frac{2}{K+2} \left(\frac{\partial U}{\partial x} + \frac{\partial V}{\partial y} \right) \right], \\ s_{3y} &= \tau p \left[U \frac{\partial U}{\partial y} + V \left(\frac{\partial V}{\partial x} + 2V \frac{\partial V}{\partial y} \right) - \frac{2}{K+2} U \left(\frac{\partial U}{\partial x} + \frac{\partial V}{\partial y} \right) + \frac{K+4}{4} \frac{\partial}{\partial y} \left(\frac{1}{\lambda} \right) \right], \\ s_{4y} &= \tau p \frac{\partial Z}{\partial y}. \end{aligned}$$

Remark 2.1 *The gas-kinetic method in [26] can completely recover the macroscopic internal energy for a perfect gas. More specifically, the flow internal energy $\frac{1}{2}\rho\frac{K+2}{2\lambda}$ is exactly recovered to be $\frac{p}{\gamma-1}$ through $p = \frac{\rho}{2\lambda}$ and $K = \frac{5-3\gamma}{\gamma-1} + 1$, where K is equal to the total number of degree of freedom of the internal variable ξ for a perfect gas, as $\gamma = (n+2)/n$ with n being the degree of molecular freedom. However, in the mixing layers, the relationship of $\gamma = (n+2)/n$ may not be maintained, and hence, $\frac{5-3\gamma}{\gamma-1}$ could be no longer an integer. Thus, the total number of degree of freedom of the internal variable ξ may not be equal to $\frac{5-3\gamma}{\gamma-1} + 1$ anymore. Consequently, this could lead to the flow in the interfacial region like a real gas.*

3 An efficient second-order γ -model BGK scheme on unstructured meshes

In this section, we present an efficient second-order gas-kinetic scheme on unstructured meshes for compressible multicomponent flows. First, we notice that the general solution f of (2.1) at any point $\vec{x} = (x, y)$ and time t is given by

$$f(x, y, t, u, v) = \frac{1}{\tau} \int_0^t g(x', y', t', u, v) e^{-(t-t')/\tau} dt' + e^{-t/\tau} f_0(x - ut, y - vt), \quad (3.1)$$

where $x' = x - u(t - t')$, $y' = y - v(t - t')$ and f_0 is the initial distribution function.

Let Ω_j denote a mesh cell with edges e_k . The cell averaged conservative variables on the cell Ω_j at the n th time level are denoted by

$$w_j^n = (\rho_j^n, \rho_j^n U_j^n, \rho_j^n V_j^n, E_j^n, \rho_j^n Z_j^n), \quad (3.2)$$

and the slopes of the conservative variables in the cell j at the n th time level in the normal direction of the three cell edges by (cf. Fig.1)

$$s_{j,j-3/2}^n, \quad s_{j,j-1/2}^n, \quad s_{j,j+1/2}^n. \quad (3.3)$$

Taking moments to the BGK equation (2.3) with $f = g$ and integrating the resulting equation over the cell Ω_j , we get

$$\int_{\Omega_j} \int \psi_\alpha (g_t + ug_x + vg_y) d\Xi dX = 0, \quad \alpha = 1, \dots, 5,$$

where $dX = dx dy$, that is

$$\frac{d}{dt} \int_{\Omega_j} \int \psi_\alpha g d\Xi dX + \int_{\Omega_j} \int (ug_x + vg_y) d\Xi dX = 0,$$

which gives

$$\frac{d}{dt} \int_{\Omega_j} \int \psi_\alpha g d\Xi dX + \sum_{e_k \in \partial\Omega_j} \int \psi_\alpha g \vec{u} \cdot n d\Xi dS = 0, \quad (3.4)$$

where $\vec{u} = (u, v)^T$, e_k is an edge of the cell Ω_j and n denotes the unit outward normal to e_k . We write (3.4) in the form of numerical fluxes as follows:

$$\frac{d}{dt} \int_{\Omega_j} \int \psi_\alpha g d\Xi dX + \sum_{e_k \in \partial\Omega_j} \mathcal{F}_{\psi_\alpha, e_k}(t) |e_k| = 0, \quad \alpha = 1, \dots, 5, \quad (3.5)$$

where $|e_k|$ is the measure of e_k and $\mathcal{F}_{\psi_\alpha, e_k}$ is the numerical flux function across the cell edge e_k corresponding to the moment ψ_α . The fully discrete form of the corresponding macroscopic flow equations of (3.5) reads then

$$w_j^{n+1} = w_j^n - \int_{t_n}^{t_{n+1}} \sum_{e_k \in \partial\Omega_j} \mathcal{F}_{w, e_k}(t) |e_k| / |\Omega_j|, \quad (3.6)$$

where $|\Omega_j|$ is the measure of Ω_j .

Therefore, our numerical algorithm can be described as follows:

Given the cell averaged value w_j^n , and the slopes $s_{j,j-3/2}^n, s_{j,j-1/2}^n, s_{j,j+1/2}^n$ in the normal direction of the

cell edges at the n th time level (Set $s_{j,j-3/2}^n = s_{j,j-1/2}^n = s_{j,j+1/2}^n = 0$, when $n = 0$). Find w_j^{n+1} , $s_{j,j-3/2}^{n+1}$, $s_{j,j-1/2}^{n+1}$, $s_{j,j+1/2}^{n+1}$ at the $(n+1)$ th time level.

Next, based on the γ -BGK model, we construct the numerical fluxes \mathcal{F}_{w,e_k} in order to obtain w_j^{n+1} by (3.6). Roughly speaking, the numerical fluxes \mathcal{F}_{w,e_k} are obtained based on the construction of an efficient 2nd-order γ -BGK solver in the normal direction of the edge e_k .

We begin with rewriting (3.6) in componentwise:

$$\left\{ \begin{array}{l} \rho_j^{n+1} = \rho_j^n - \int_{t_n}^{t_{n+1}} \sum_{e_k \in \partial\Omega_j} \mathcal{F}_{\rho,e_k}(t) |e_k| / |\Omega_j|, \\ (\rho U)_j^{n+1} = (\rho U)_j^n - \int_{t_n}^{t_{n+1}} \sum_{e_k \in \partial\Omega_j} \mathcal{F}_{\rho U,e_k}(t) |e_k| / |\Omega_j|, \\ (\rho V)_j^{n+1} = (\rho V)_j^n - \int_{t_n}^{t_{n+1}} \sum_{e_k \in \partial\Omega_j} \mathcal{F}_{\rho V,e_k}(t) |e_k| / |\Omega_j|, \\ E_j^{n+1} = E_j^n - \int_{t_n}^{t_{n+1}} \sum_{e_k \in \partial\Omega_j} \mathcal{F}_{E,e_k}(t) |e_k| / |\Omega_j|, \\ (\rho Z)_j^{n+1} = (\rho Z)_j^n - \int_{t_n}^{t_{n+1}} \sum_{e_k \in \partial\Omega_j} \mathcal{F}_{\rho Z,e_k}(t) |e_k| / |\Omega_j|. \end{array} \right. \quad (3.7)$$

The first stage is to reconstruct the initial distribution function f_0 by using the values w_j^n of the macroscopic conservative variables. f_0 will be needed in the dynamical evolution stage below (the second stage) for the computation of the gas distribution function f at a cell interface (cf. (3.1)).

By rotating the coordinates, we may assume the interface between the cell j and the cell $j+1$ to be $\Gamma_{j+1/2} := \{(x_{j+1/2}, y); -a < y < a\}$ for some $a > 0$ (see Fig.1), and without loss of generality we may take $x_{j+1/2} = 0$. For a compressible flow, the initial gas distribution f_0 at time $t = 0$ is supposed to have the form

$$f_0 = \begin{cases} g^l [1 + a^l x - \tau(a^l u + A^l)], & x \leq 0, \\ g^r [1 + a^r x - \tau(a^r u + A^r)], & x \geq 0. \end{cases} \quad (3.8)$$

The equilibrium state g around $(x = 0, y = 0, t = 0)$ is assumed to be

$$g = g_0 [1 + (1 - H(x))\bar{a}^l x + H(x)\bar{a}^r x] + \bar{A} t, \quad (3.9)$$

where $H(x)$ is the Heaviside function, g_0 is a local Maxwellian distribution located at $x = 0$, g and g_0 have the same expression as that in (2.4). The coefficients $a^{l,r}$, $\bar{a}^{l,r}$, $A^{l,r}$, \bar{A} in (3.8) and (3.9) are related to the derivatives of the Maxwellian in space and time, and assumed to have the following form obtained from a Taylor expansion of the Maxwellian:

$$\begin{aligned} a^{l,r} &= a_1^{l,r} + a_2^{l,r} u + a_3^{l,r} v + \frac{1}{2} a_4^{l,r} (u^2 + v^2 + \xi^2) + a_5^{l,r} z, \\ \bar{a}^{l,r} &= \bar{a}_1^{l,r} + \bar{a}_2^{l,r} u + \bar{a}_3^{l,r} v + \frac{1}{2} \bar{a}_4^{l,r} (u^2 + v^2 + \xi^2) + \bar{a}_5^{l,r} z, \\ A^{l,r} &= A_1^{l,r} + A_2^{l,r} u + A_3^{l,r} v + \frac{1}{2} A_4^{l,r} (u^2 + v^2 + \xi^2) + A_5^{l,r} z, \\ \bar{A} &= \bar{A}_1 + \bar{A}_2 u + \bar{A}_3 v + \frac{1}{2} \bar{A}_4 (u^2 + v^2 + \xi^2) + \bar{A}_5 z, \end{aligned}$$

where $a_j^{l,r}$, $\bar{a}_j^{l,r}$, $A_j^{l,r}$ and \bar{A}_j can be determined by using the relation between the macroscopic variables and the gas distribution function in the same manner as in [25], the known cell averaged values (3.2) and

slopes (3.3). For example, the coefficients a_j^l can be obtained by the following identity:

$$\int \begin{pmatrix} 1 \\ u \\ v \\ \frac{1}{2}(u^2 + v^2 + \xi^2) \\ z \end{pmatrix} \left(a_1 + a_2 u + a_3 v + \frac{1}{2} a_4 (u^2 + v^2 + \xi^2) + a_5 z \right) g d\Xi = \begin{pmatrix} \frac{\partial \rho}{\partial n} \\ \frac{\partial \rho \bar{U}}{\partial n} \\ \frac{\partial \rho \bar{V}}{\partial n} \\ \frac{\partial E}{\partial n} \\ \frac{\partial \rho Z}{\partial n} \end{pmatrix}, \quad (3.10)$$

where

$$\tilde{U} = U \cos \phi + V \sin \phi, \quad \tilde{V} = -U \sin \phi + V \cos \phi,$$

and ϕ is the angle of the normal direction, $\frac{\partial}{\partial n}$ is the differentiation in the normal direction of the cell interface between the cell j and the cell $j+1$ at the n th time level which is known and given by (3.3). The coefficients A_j^l can be computed by the compatibility conditions:

$$\int (a^l u + A^l) \psi_\alpha g^l d\Xi = 0, \quad \alpha = 1, \dots, 5,$$

and the coefficients \bar{A}_j^l by the conservative constraints over a time step:

$$\int_0^{\Delta t} \int (g - f) \psi_\alpha dt d\Xi = 0, \quad \alpha = 1, \dots, 5.$$

In this way, all unknown terms on the right-hand side of (3.8) and (3.9) can be determined. So, f_0 and g are obtained.

Inserting g and f_0 into (3.1) and recalling the definition of $H(x)$, we obtain the gas distribution function f at the cell interface $\Gamma_{j+1/2}$

$$\begin{aligned} f(x_{j+1/2}, t, u, v, \xi) &= (1 - e^{-t/\tau}) g_0 + \left[\tau(-1 + e^{-t/\tau}) + t e^{-t/\tau} \right] [\bar{a}^l H(u) + \bar{a}^r (1 - H(u))] u g_0 \\ &+ \tau \left(\frac{t}{\tau} - 1 + e^{-t/\tau} \right) \bar{A} g_0 + e^{-t/\tau} (1 - u t a^l) H(u) g^l \\ &+ e^{-t/\tau} (1 - u t a^r) (1 - H(u)) g^r + e^{-t/\tau} \left(-\tau A^l H(u) g^l - \tau A^r (1 - H(u)) g^r \right), \end{aligned}$$

from which the fluxes across the cell interface $\Gamma_{j+1/2}$ are given then by

$$\begin{pmatrix} \mathcal{F}_{\rho, e_k} \\ \mathcal{F}_{\rho \bar{U}, e_k} \\ \mathcal{F}_{\rho \bar{V}, e_k} \\ \mathcal{F}_{E, e_k} \\ \mathcal{F}_{\rho Z, e_k} \end{pmatrix} = \int u \begin{pmatrix} 1 \\ u \\ v \\ \frac{1}{2}(u^2 + v^2 + \xi^2) \\ z \end{pmatrix} f(x_{j+1/2}, 0, t, u, v, \xi) d\Xi.$$

Therefore, the numerical fluxes in the normal direction across the interface e_k between the cell j and the cell $j+1$ (cf. Fig.1) can be written as

$$\begin{pmatrix} \mathcal{F}_{\rho, e_k} \\ \mathcal{F}_{\rho U, e_k} \\ \mathcal{F}_{\rho V, e_k} \\ \mathcal{F}_{E, e_k} \\ \mathcal{F}_{\rho Z, e_k} \end{pmatrix} = \begin{pmatrix} \mathcal{F}_{\rho, e_k} \\ \mathcal{F}_{\rho \bar{U}, e_k} \cos \phi - \mathcal{F}_{\rho \bar{V}, e_k} \sin \phi \\ \mathcal{F}_{\rho \bar{U}, e_k} \sin \phi + \mathcal{F}_{\rho \bar{V}, e_k} \cos \phi \\ \mathcal{F}_{E, e_k} \\ \mathcal{F}_{\rho Z, e_k} \end{pmatrix}. \quad (3.11)$$

Finally, we use (3.7) and (3.11) to obtain the value of the conservative variables w_j^{n+1} at the $(n+1)$ th time level.

To finish the description of our algorithm, it remains to construct the slopes $s_{j,j-3/2}^{n+1}$, $s_{j,j-1/2}^{n+1}$, $s_{j,j+1/2}^{n+1}$ for each cell. We should point out here that in the construction of our scheme, the crucial point is that one can extract more information (e.g., the value of the conservative variables at the points $\vec{x}_{j-3/2}$, $\vec{x}_{j-1/2}$, $\vec{x}_{j+1/2}$ on the cell boundary) from the two neighboring gas distribution functions (see Fig.1), from which we can therefore evaluate not only the numerical fluxes but also the slopes $s_{j,j-3/2}^{n+1}$, $s_{j,j-1/2}^{n+1}$, $s_{j,j+1/2}^{n+1}$. That means, we can use the information in a cell only to construct the slopes at cell interfaces. This avoids using the values of the conservative variables from the neighboring cells in the construction of the slopes, and therefore, the scheme is computationally cheap and efficient. As is well-known, it is sometimes very difficult to choose a suitable stencil to construct the slopes of w_j^{n+1} on unstructured meshes.

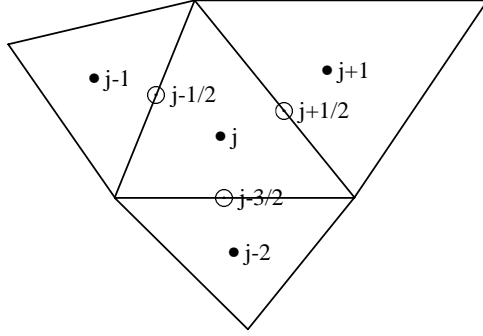


Figure 1: Slope update: dots are the centroids, circles are the interface points

To get the slopes, we first note that the value of the conservative variables at the cell interface between the cell j and the cell $j+1$ at the $(n+1)$ th time level can be obtained as follows, by integrating the two half equilibrium distribution functions of the cells j (denoted by g_l) and $j+1$ (denoted by g_r) (see Fig.2).

$$\begin{aligned}
 w_{j+1/2}^{n+1} = & \int_{u < U_l} \begin{pmatrix} 1 \\ u \\ v \\ \frac{1}{2}(u^2 + v^2 + \xi^2) \\ z \end{pmatrix} g_l d\Xi + \int_{u > U_r} \begin{pmatrix} 1 \\ u \\ v \\ \frac{1}{2}(u^2 + v^2 + \xi^2) \\ z \end{pmatrix} g_r d\Xi \\
 & + \int \begin{pmatrix} 1 \\ u \\ v \\ \frac{1}{2}(u^2 + v^2 + \xi^2) \\ z \end{pmatrix} \bar{A} g_0 \Delta t d\Xi.
 \end{aligned} \tag{3.12}$$

We point out here that the construction (3.12) is different from that in [15]. Instead of the two parts on the left respectively right hand side of U_l respectively U_r of the gas distribution function f , we use here two half Maxwellians g_r, g_l . We find that this kind of construction can eliminate spurious oscillations in some cases, such as, when the velocity at a cell interface is larger than that in the neighboring cells at the next time step, the slopes constructed as in [15] could cause spurious oscillations in the vicinity of the interface. Hence, we use here the interface values given by (3.12) to remove possible oscillations near the cell interface.

Consequently, the slopes of the conservative variables w_j^{n+1} in the cell j at time step t_{n+1} in the normal direction of the cell interface between the cell j and the cell $j+1$ can be obtained by taking

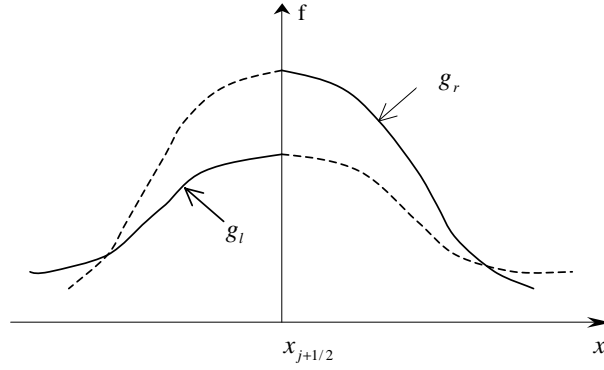


Figure 2: Value of the flow variables at an interface: obtained by using two half Maxwellians of the cells j (denoted by g_i) and $j + 1$ (denoted by g_r)

appropriate differences directly and using a limiter. Let

$$s_{j,j+1/2}^+ = (w_{j+1/2}^{n+1} - w_j^{n+1})/dn_+, \quad s_{j,j+1/2}^- = (w_j^{n+1} - \bar{w}^{n+1})/dn_-,$$

where \bar{w}^{n+1} is the average of $w_{j-1/2}^{n+1}$ and $w_{j-3/2}^{n+1}$, dn_+ is the projection of $d_{j,j+1/2}$ in the normal direction, and dn_- is the projection of $d_{j,j-1/2}$ in the normal direction, $d_{j,j+1/2}$ is the distance from the centroid of the cell j to the interface point $j + 1/2$, $d_{j,j-1/2}$ is the distance from the centroid of the cell j to the center between the interface points $j - 1/2$ and $j - 3/2$.

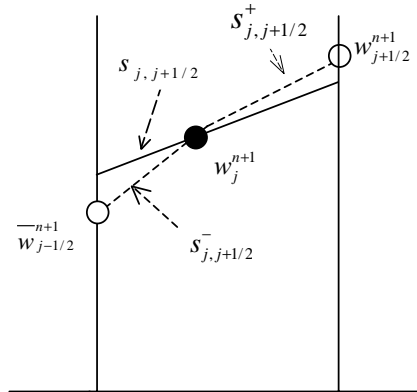


Figure 3: Slope $s_{j,j+1/2}$ for the cell j in the normal direction of the interface between the cells j and $j + 1$

Having had the slopes $s_{j,j+1/2}^\pm$, thus we can use van Leer's limiter to obtain easily the slope $s_{j,j+1/2}^{n+1}$ of the conservative variables in the cell j in the normal direction of the cell interface between the cell j and the cell $j + 1$, see Fig.3. The slopes in the other two normal directions for the cell j can be obtained in the same manner.

In summary, our numerical algorithm consists of three steps:

(1) *Initial reconstruction*: Use the cell averaged values of the conservative variables w_j and limiters to get the linearly interpolated values \bar{w}_j .

(2) *Gas evolution stage*: Use the initial data reconstructed from the first step to give an explicit solution of the BGK model (2.3). More precisely, one constructs the initial distribution function f_0 and

the equilibrium state g from the reconstructed initial data, and thus obtains the general explicit solution of the BGK model (2.3), from which one gets the numerical fluxes across cell interfaces.

(3) *Construction of the slopes*: Use the information in a cell only to construct the slopes of the conservative variables in the normal direction of a cell interface.

4 Numerical examples

We now present three numerical examples, one one-dimensional and two two-dimensional multifluid problems to demonstrate our scheme. In all the cases, the numerical time step is taken as

$$\Delta t = CFL \sqrt{|\Omega|} / (\max |u| + C),$$

where CFL is the CFL number and C is the sound speed. In the following numerical examples, we take $CFL = 0.25 \sim 0.45$.

EXAMPLE 1. Sod's Shock-Tube Problem

This problem has been extensively studied (see, e.g., [9, 25]). It is a one-dimensional shock tube problem with two different initial constant states in a tube with unit length:

$$\begin{aligned} (\rho_l = 1, \rho_l U_l = 0, E_l = 2.5, \gamma_l = 1.4), \\ (\rho_r = 0.125, \rho_r U_r = 0, E_r = 0.5, \gamma_r = 1.2), \end{aligned}$$

and the initial discontinuity is located at $x = 1/2$. The computation is carried out on a uniform mesh with 200 cells. The numerical results obtained using our efficient second-order scheme and the first-order scheme are shown in Fig.5 and Fig.6 for the density and gamma. We see that the numerical results obtained using the second-order scheme are generally in good agreement with the corresponding ones given in [9, 25] using different schemes. Comparing our numerical results with the exact solution, the second order scheme resolves obviously better than the first order scheme. In Fig.7 and 8 the computed results by the second-order scheme with 200 and 400 cells are compared. We clearly see that as the grid is getting refined, the numerical solution tends to the exact one.

EXAMPLE 2. High Pressure Problem

This problem is taken from Abgrall's paper [1] with initial data

$$\begin{aligned} (\rho_l = 14.54903, \rho_l U_l = 0.0, E_l = 2.9e7, \gamma_l = 1.67), \\ (\rho_r = 1.16355, \rho_r U_r = 0.0, E_r = 2.5e5, \gamma_r = 1.4). \end{aligned}$$

From the numerical test point of view, this problem is difficult for multicomponent flow solvers due to its large pressure variation, and is a good test for the accuracy and robustness of a scheme. Here in the computation 1200 cells are used. The simulated results for the density, gamma, velocity and pressure are shown in Fig.9–Fig.12, respectively. We see that comparing with the “exact” solution, our numerical scheme is quite accurate. Moreover, the velocity and pressure are obviously smoother across the material interface than those in [1].

EXAMPLE 3. A Mach 1.22 Shock Hits a R22 Cylindrical Bubble (see e.g. [12])

We examine the interaction of a Mach 1.22 planar shock wave with a R22 cylindrical bubble. A schematic description of computational set-up can be found in [10], the initial flow distribution is determined from the standard shock relation with the given strength of the incident shock wave. The bubble is assumed to be in both thermal and mechanical equilibrium with the surrounding air. The non-dimensionalized initial conditions are

$$\begin{aligned}
W &= (\rho = 1, U = 0, V = 0, P = 1, \gamma = 1.4), \text{ pre-shock air,} \\
W &= (\rho = 1.3764, U = 0.394, V = 0, P = 1.5698, \gamma = 1.4), \text{ post-shock air,} \\
W &= (\rho = 3.1538, U = 0, V = 0, P = 1, \gamma = 1.249), \text{ R22,}
\end{aligned}$$

the reflection boundary conditions on the upper and lower boundaries are used. In the computation 105852 triangular cells with 53446 nodes are used. The results are shown in Fig.13 where the contours of the density are given at three different times. The space-time location of the refraction wave, shock wave, and transmitted wave, downstream and upstream edges of the bubble are shown in the Fig.4.

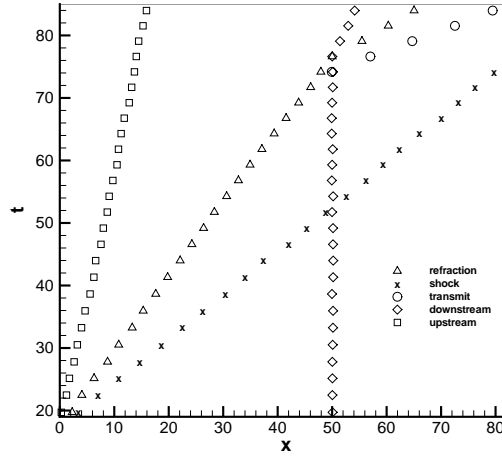


Figure 4: Space-time location of the refraction wave, shock wave, and transmitted wave, downstream and upstream edges of the bubble

Table 1. Velocity Comparison for R22 Bubble Test

Velocity(m/s)	V_s	V_r	V_t	V_d	V_u
Experiment	415	240	540	78	73
Quirk&Karni	420	254	560	116	74
BGK	409.	242	550	90	72

Since the initial data are non-dimensionalized, in order to give a quantitative comparison for the velocity, we have to compute the sound speed C . Recalling that $\rho_\infty = 1.225 \text{ kg/m}^2$, $P_\infty = 1.0101325 \times 10^5 \text{ Pa}$, we easily find that

$$C = \sqrt{\gamma P_\infty / \rho_\infty} = 288.07 \text{ m/s.}$$

So, we can get the physical velocity V^* from the numerical velocity V by utilizing the relation $V^* = V \times C$. In Table 1, we give a quantitative comparison of the velocity obtained by the γ -model

BGK scheme with the experimental data and the numerical results obtained by Quirk and Karni [20]. From the table we easily see that the computed results by the γ -model BGK scheme are in very good agreement with the experimental data and closer to the experiment than those in [20]. We also mention that in [23] Shyue presented similar numerical results. However, Shyue used much more cells (3650×365) than ours in his computation.

EXAMPLE 4. A Mach 1.22 Shock Hits a Helium Cylindrical Bubble (see e.g. [20, 12])

We consider the interaction of a Mach 1.22 planar shock wave with a cylindrical helium bubble. We use the same grid as in Example 3, i.e., 105852 triangular cells with 53446 nodes. The bubble is assumed to be in both thermal and mechanical equilibrium with the surrounding air. The non-dimensionalized initial conditions are

$$\begin{aligned} W &= (\rho = 1, U = 0, V = 0, P = 1, \gamma = 1.4), \quad \text{pre-shock air,} \\ W &= (\rho = 1.3764, U = 0.394, V = 0, P = 1.5698, \gamma = 1.4), \quad \text{post-shock air,} \\ W &= (\rho = 0.1358, U = 0, V = 0, P = 1, \gamma = 1.67), \quad \text{helium,} \end{aligned}$$

the reflection boundary conditions on the upper and lower boundaries are used. The results are shown in Fig.14 where the contours of the density are given at three different times.

From Examples 3 and 4, it is easy to see that the numerical results obtained using the scheme of this paper reproduce the large-scale structure of the corresponding results in [20, 4, 12] and of the experiments described in [5].

5 Conclusion

In this paper, based on the γ -model, the BGK scheme and the time-dependent gas distribution function, we present an efficient second-order gas-kinetic BGK scheme for compressible multicomponent flows on unstructured meshes. The second-order accuracy of the scheme is achieved by including slopes of the flow variables, the initial distribution function and the equilibrium state in the reconstruction step, and the efficiency lies in the fact that the slopes in a cell are constructed by using the information within the cell only. Using the explicitly constructed time-dependent gas distribution function, we can obtain in addition the values of the flow variables at cell edges of the cell, which together with the cell averaged values make it possible to construct the slopes of the flow variables in the cell, avoiding the use of the values from neighboring cells in the usual process. Thus, with the stencil of a first-order scheme, we have constructed a second-order gas-kinetic scheme. Several numerical results obtained using the scheme of this paper are presented which are compared with either the exact and benchmark solutions or the experimental data. The comparison demonstrates the accuracy and efficiency of the scheme.

Acknowledgement. This work was supported by the National Basic Research Program (Grant No. 2005CB321700), NSFC (Grant No. 10225105) and a CAEP fund (No. 20060644).

References

- [1] R. Abgrall, How to prevent pressure oscillations in multicomponent flow calculation: A quasi conservative approach. *J. Comput. Phys.* **125** (1996), 150-160.
- [2] P.L. Bhatnagar, E.P. Gross and M. Krook, A model for collision processes in gases I: Small amplitude processes in charged and neutral one component systems. *Phys. Rev.* **94** (1954), 511-525.
- [3] S. Chapman and T.G. Cowling, *The Mathematical Theory of Non-Uniform Gases*. Cambridge Univ. Press (1990).

- [4] R.P. Fedkiw, T. Aslam, B. Merriman and S. Osher, A non-oscillatory Eulerian approach to interfaces in multi material flows (The Ghost Fluid Method). *J. Comput. Phys.* **152** (1999), 457-492.
- [5] J.F. Haas and B. Sturtevant, Interactions of weak shock waves with cylindrical and spherical gas inhomogeneities. *J. Fluid Mechanics* **181** (1987), 41-76.
- [6] X.Y. He and L.S. Luo, Theory of the lattice Boltzmann method: From the Boltzmann equation to the lattice Boltzmann equation. *Phys. Rev. E* **56** (6) (1997), 6811-6817.
- [7] S. Jiang and G. Ni, A γ -model BGK scheme for compressible multifluids, *Int. J. Numer. Meth. Fluids* **46** (2004), 163-182.
- [8] S. Jiang and G. Ni, A second order γ -model BGK scheme for multimaterial compressible flows, *Appl. Numer. Math.* **57** (2007), 579-608.
- [9] S. Karni, Multicomponent flow calculations by a consistent primitive algorithm. *J. Comput. Phys.* **112** (1994), 31-43.
- [10] S. Karni, Hybrid multifluid algorithms. *SIAM J. Sci. Comput.* **17** (1997), 1019-1039.
- [11] C. Kim and A. Jameson, A robust and accurate LED-BGK solver on unstructured adaptive meshes. *J. Comput. Phys.* **143** (1998), 598-627.
- [12] Y.S. Lian and K. Xu, Gas-kinetic scheme for multimaterial flows and its application in chemical reactions. *J. Comput. Phys.* **163** (2000), 349-375.
- [13] G. May and A. Jameson, Unstructured algorithm for the inviscid and viscous flows embedded in a unified solver architecture: Flo3xx. *AIAA Paper* 2005-0318, 2005.
- [14] G. May, B. Srinivasan and A. Jameson, An improved gas-kinetic BGK finite volume method for three dimensional transonic flow. *J. Comput. Phys.* **220** (2007), 856-878.
- [15] G. Ni, S. Jiang and K. Xu, Efficient kinetic schemes for steady and unsteady flow simulations on unstructured meshes. *J. Comput. Phys.* (accepted for publication)
- [16] T. Ohwada, On the construction of kinetic scheme. *J. Comput. Phys.* **177** (2002), 156-175.
- [17] K.H. Prendergast and K. Xu, Numerical hydrodynamics from gas kinetic theory. *J. Comput. Phys.* **109** (1993), 53-66.
- [18] D.I. Pullin, Direct simulation methods for compressible inviscid ideal gas flow. *J. Comput. Phys.* **34** (1980), 231-244.
- [19] J. Quirk, A contribution to the great Riemann solver debate. *Int. J. Numer. Meth. Fluids* **18** (1994), 555-574.
- [20] J.J. Quirk and S. Karni, On the dynamics of a shock bubble interaction, *J. Fluid Mech.* **318**, (1996), 129-163.
- [21] P.L. Roe, A new approach to computing discontinuous flow of several ideal gases. Technical Report (Cranfield Institute of Technology 1984).
- [22] K.M. Shyue, An efficient shock capturing algorithm for compressible multicomponent problems. *J. Comput. Phys.* **142** (1998), 208-242.
- [23] K.M. Shyue, A wave propagation based volume tracking method for compressible multicomponent flow in two space dimension. *J. Comput. Phys.* **215** (2006), 219-244.

- [24] K. Xu and K.H. Prendergast, Numerical Navier-Stokes solutions from gas kinetic theory. *J. Comput. Phys.* **114** (1994), 9-17.
- [25] K. Xu, Gas Kinetic Scheme for Unsteady Compressible Flow Simulations. *Von Kármán Institute for Fluid Dynamics, Lecture Note Series* 1998-03 (1998).
- [26] K. Xu, A gas-kinetic BGK scheme for the Navier-Stokes equations and its connection with artificial dissipation and Godunov method. *J. Comput. Phys.* **171** (2001), 289-335.

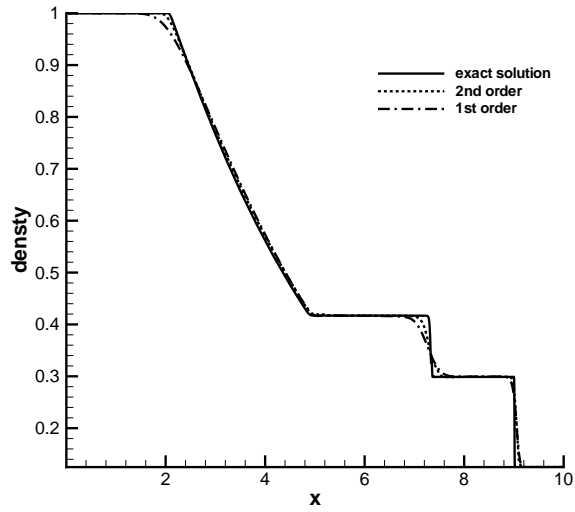


Figure 5: Sod's shock-tube problem: Density distribution, the 1st-order and efficient 2nd-order γ -model BGK schemes, the exact solution

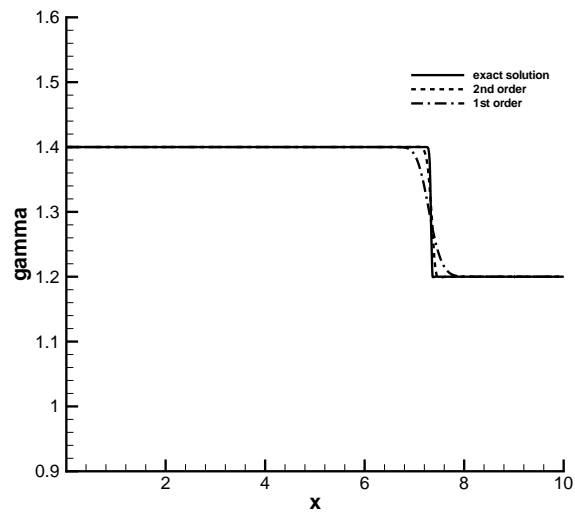


Figure 6: Sod's shock-tube problem: γ distribution, the 1st-order and efficient 2nd-order γ -model BGK schemes, the exact solution

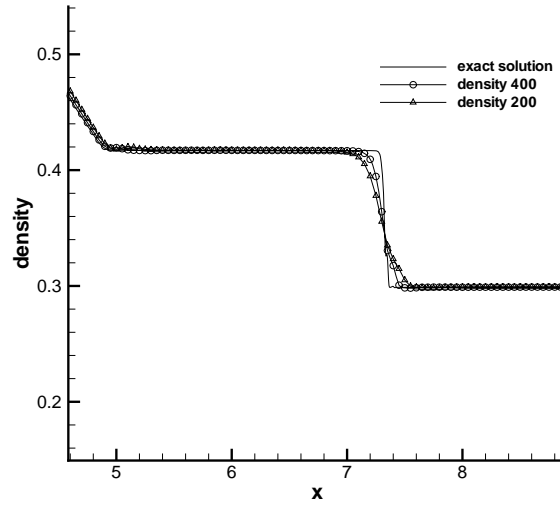


Figure 7: Sod's shock-tube problem: Density distributions computed using the 2nd-order scheme with 200 and 400 cells, compared with the exact solution

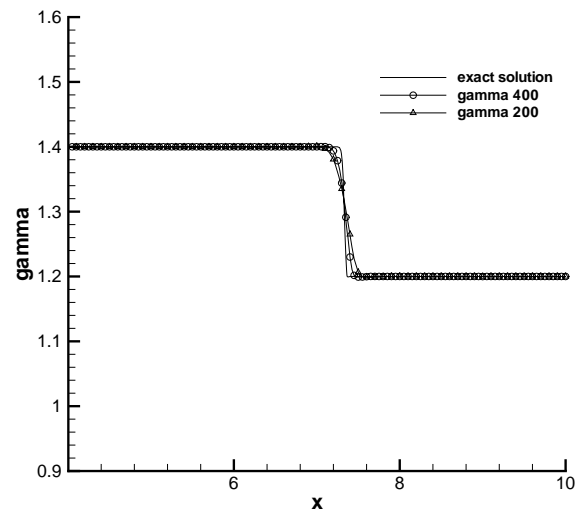


Figure 8: Sod's shock-tube problem: γ distributions computed using the 2nd-order scheme with 200 and 400 cells, compared with the exact solution

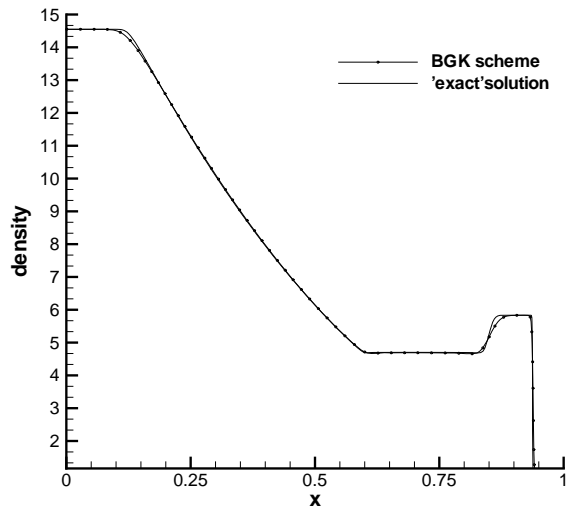


Figure 9: High pressure problem: Density distribution at time $t=0.2$

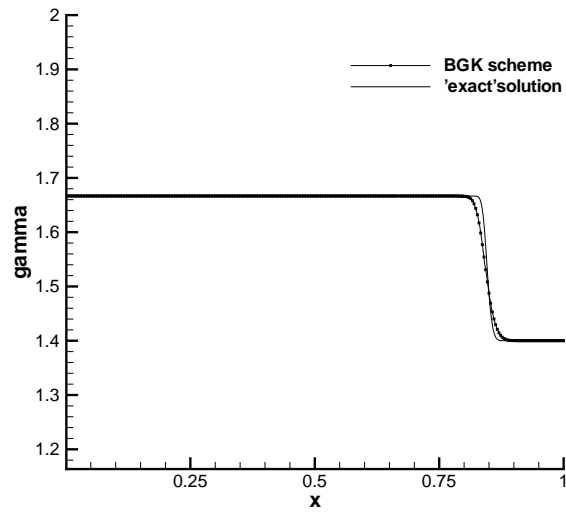


Figure 10: High pressure problem: γ distribution at time $t=0.2$

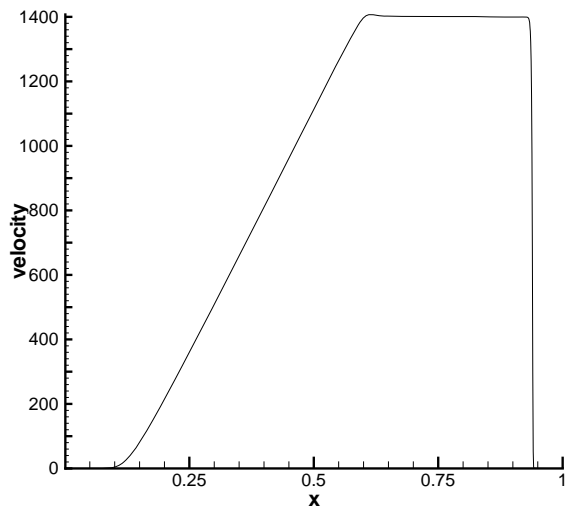


Figure 11: High pressure problem: Velocity distribution at time $t=0.2$

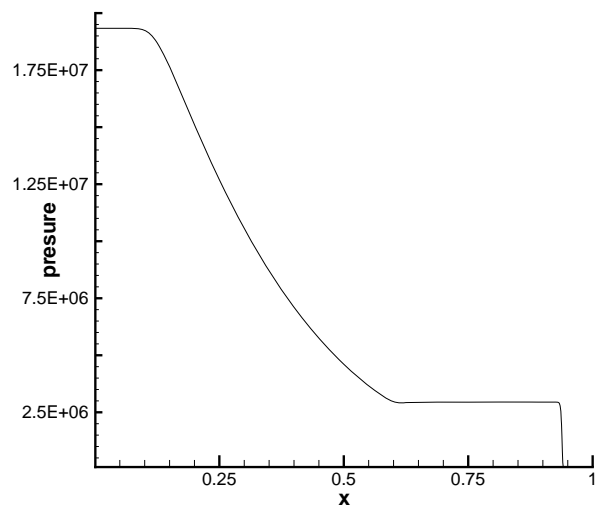


Figure 12: High pressure problem: Pressure distribution at time $t=0.2$

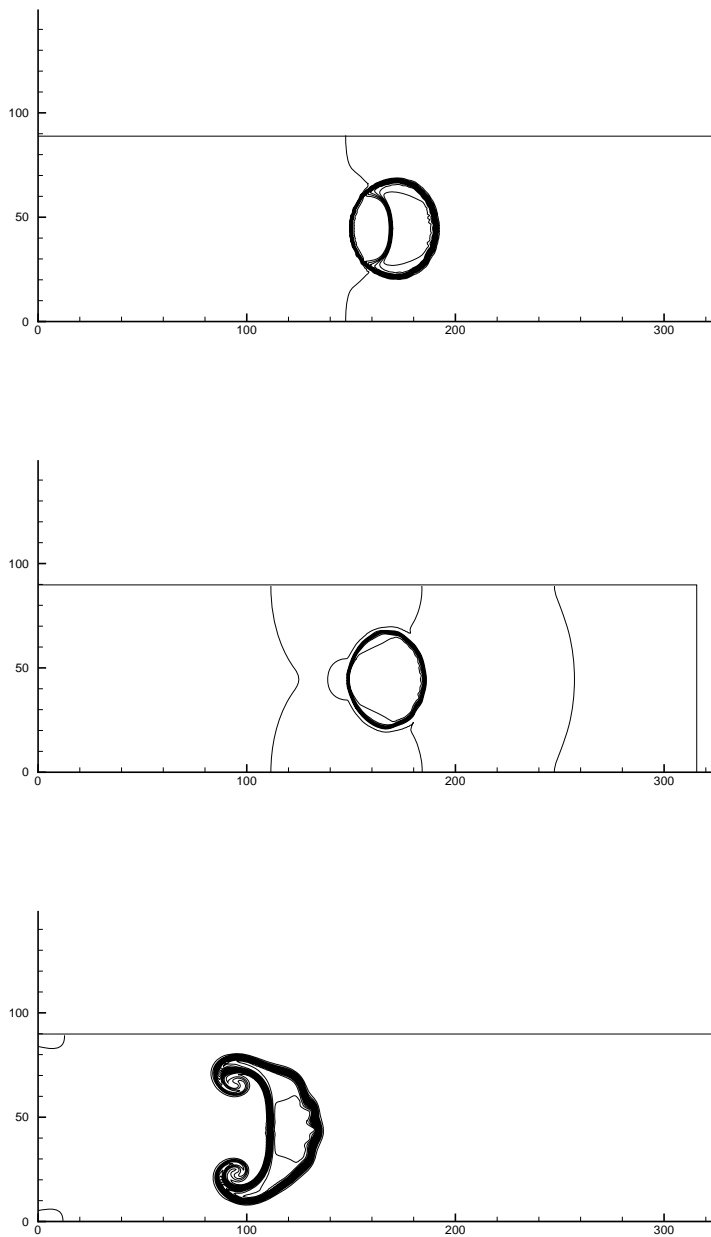


Figure 13: Interaction of a shock with a *R22* bubble: Density contours at three different times $t=28, 42, 103$. 105852 cells with 53446 nodes are used

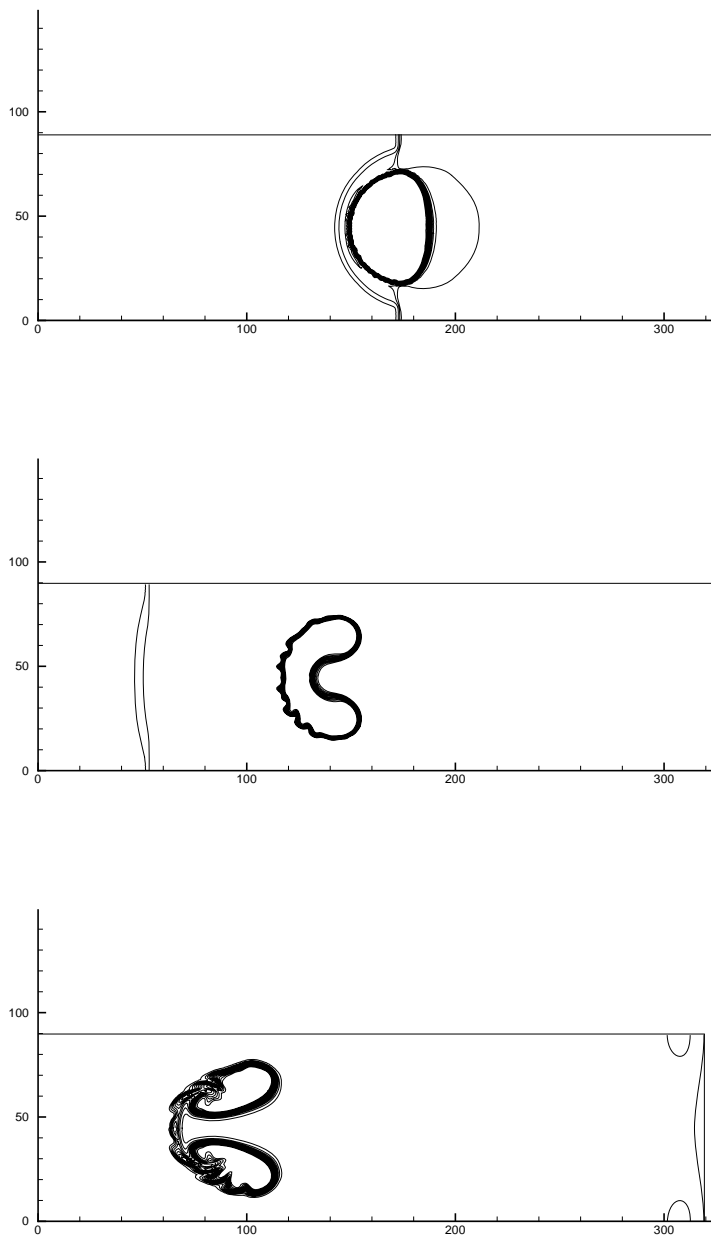


Figure 14: Interaction of a shock with a helium bubble: Density contours at three different times $t=24,125,176$. 105852 cells with 53446 nodes are used